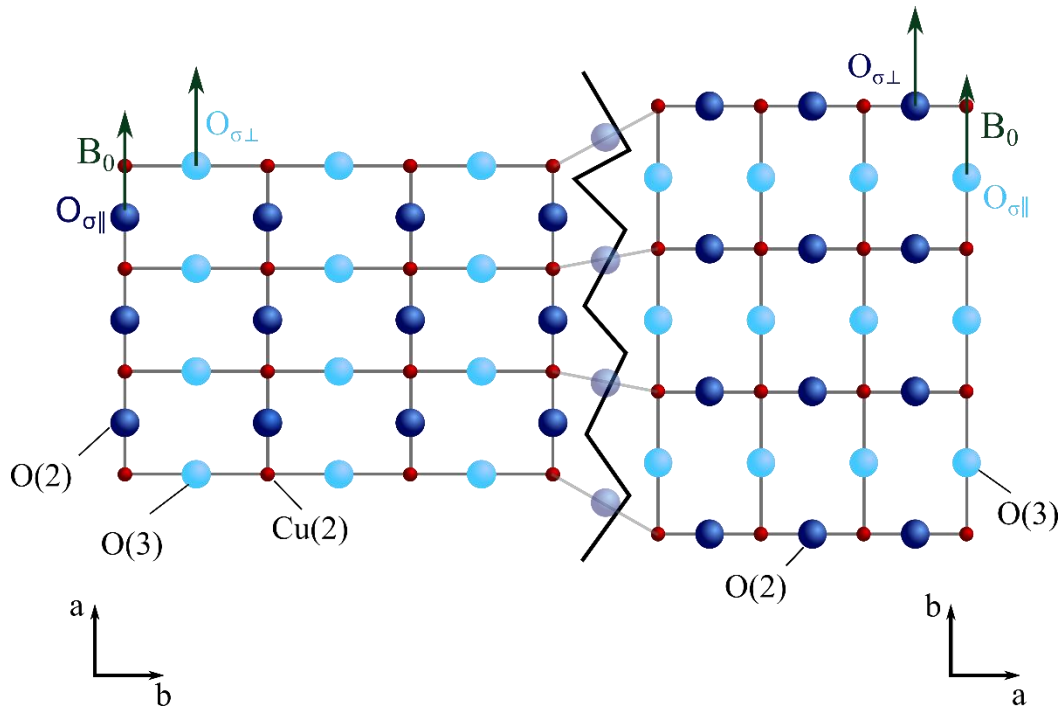
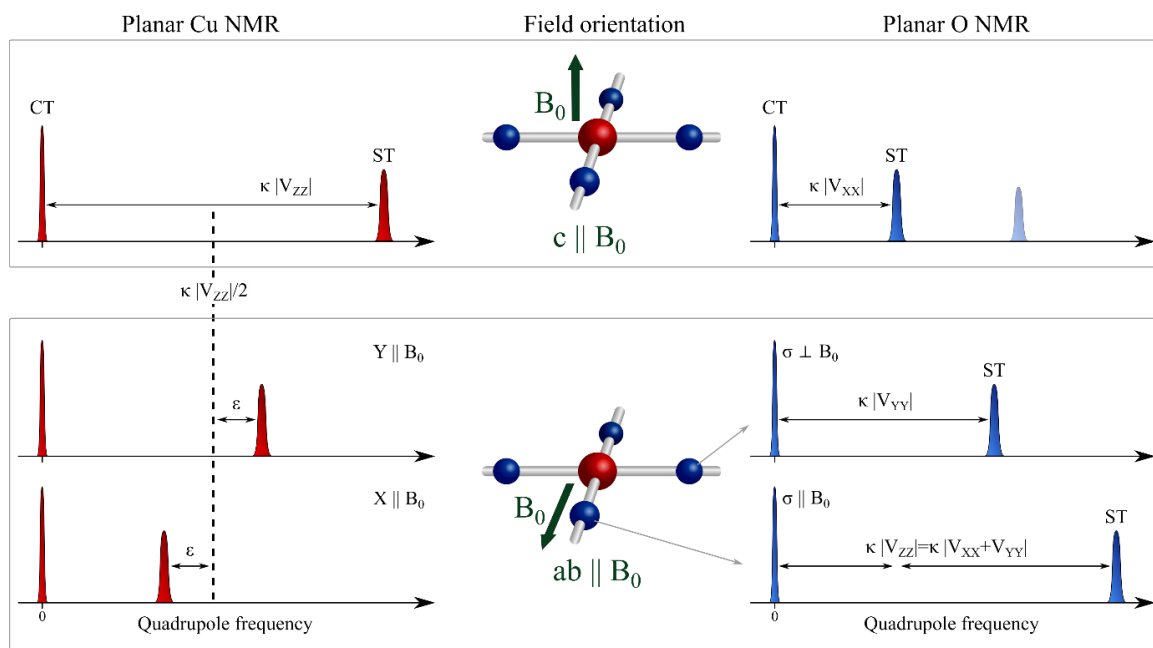


Supplementary Information



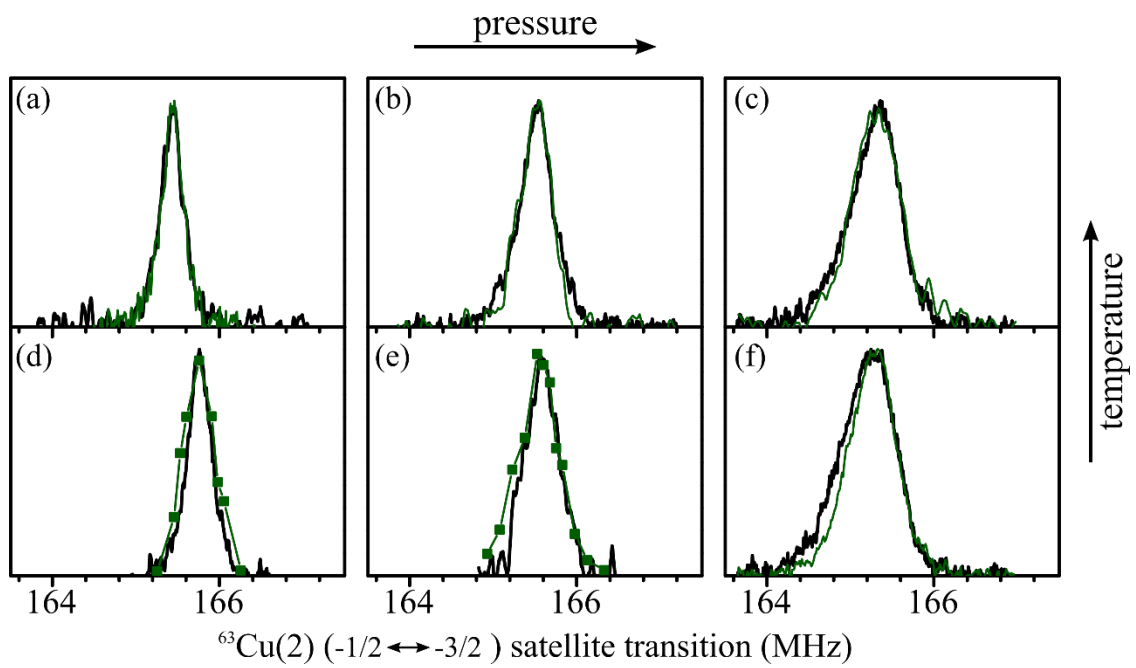
Supplementary Figure 1: Sketch of twinned, orthorhombic CuO_2 plane

Due to the CuO_y chains, the CuO_2 plane exhibit a small orthorhombicity, for $\text{YBa}_2\text{Cu}_3\text{O}_{6.9}$ of about $(a-b)/(a+b) = 8 \cdot 10^{-3}$ (increased for visualization by a factor of about 20). Twinning results in two alternating crystal phases (left and right) where the crystal axes are rotated by 90° about the crystal's c -axis. The planar copper site $\text{Cu}(2)$ has thereby a slightly non-axially symmetric environment, and for planar oxygen the different axis length result in two inequivalent sites $\text{O}(2)$ and $\text{O}(3)$. For the field perpendicular to the ab -plane ($c \parallel B_0$), NMR measures $\text{O}(2)$ and $\text{O}(3)$ simultaneously. However, with the magnetic field B_0 along either one Cu-O-Cu bond direction, NMR distinguishes O sites with their bond parallel and perpendicular to the field. Nevertheless, for a twinned crystal $\text{O}(2)$ and $\text{O}(3)$ are both measured with their bond parallel and perpendicular to the field simultaneously.



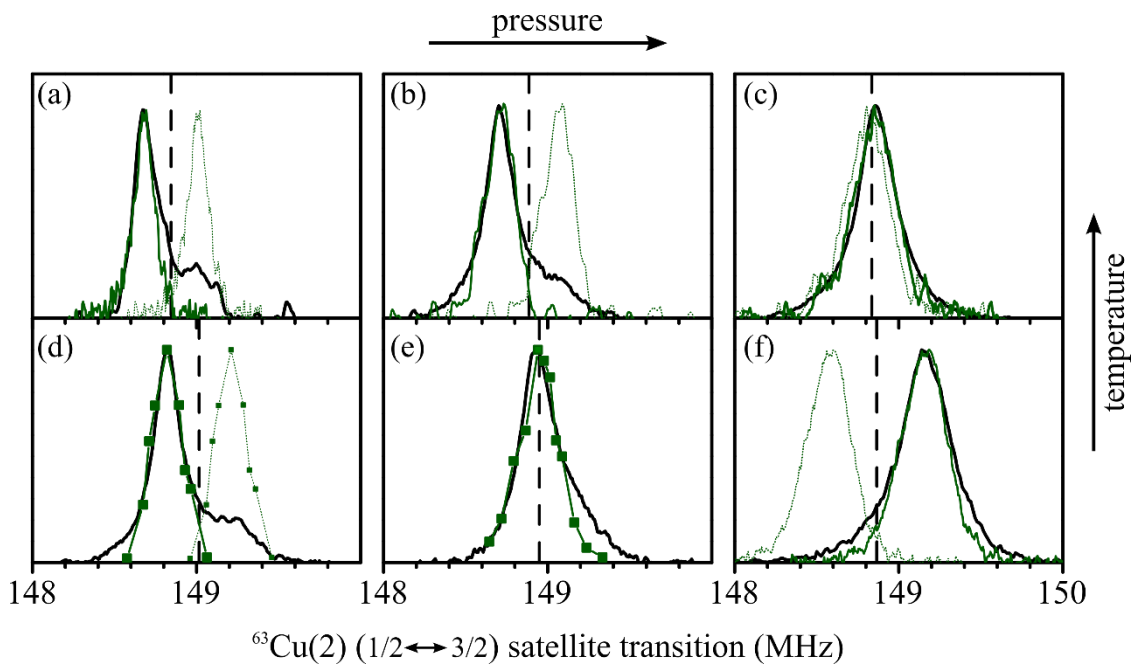
Supplementary Figure 2: Electric field gradient at planar Cu and O measured by NMR

The principle components of the planar Cu and O EFGs are measurable as frequency shifts between the central transition (CT) and the satellite transitions (ST). (left) The largest EFG principle value V_{zz} of planar Cu is measured for $c \parallel B_0$ ($\kappa = 3eQ/2I(2I-1)h$). For $ab \parallel B_0$, the satellite position of an axially symmetric EFG ($V_{xx} = V_{yy}$) is indicated by the dashed line. A small non-axial symmetry of the EFG ($V_{xx} \neq V_{yy}$) shifts the resonance from the dashed line towards higher (lower) quadrupole frequencies by $\varepsilon = \kappa |V_{xx} - V_{yy}|$ if the magnetic field is along the EFG principle axis Y (X). If both peaks are measured simultaneously, the orientation of the EFGs vary in field direction. (center) Respective magnetic field orientation illustrated at a planar CuO_4 unit. (right) The smallest O EFG principle value V_{xx} is measured for $c \parallel B_0$. With the magnetic field along either one Cu-O bond direction ($ab \parallel B_0$), V_{yy} is measured for the O having their bond perpendicular to magnetic field ($\sigma \perp B_0$) and the largest component V_{zz} is obtain for the O with the field parallel to the bond ($\sigma \parallel B_0$). Due to the traceless of the EFG, V_{zz} can also be calculated from the two other directions.



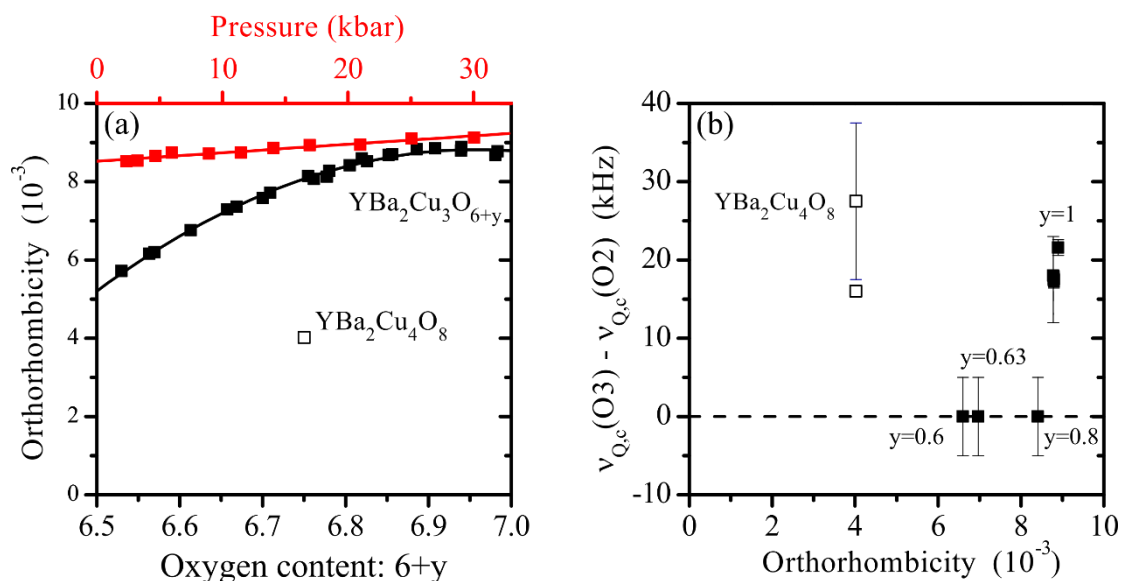
Supplementary Figure 3: Planar ^{63}Cu NQR vs. satellite spectra for $c \parallel B_0$

The upper and lower panels correspond to 300 K and 100 K, respectively, with pressures of 0 kbar (a, d), 9 kbar (b, e) and 18 kbar (c, f). The NMR ($c \parallel B_0$) satellite transitions (black) agree with simulated spectra (green) based on NQR ($B_0 = 0$) measurements, cf. Methods in main article. This shows that the largest principle value of the Cu EFG is well-defined in terms of mean value and distribution.



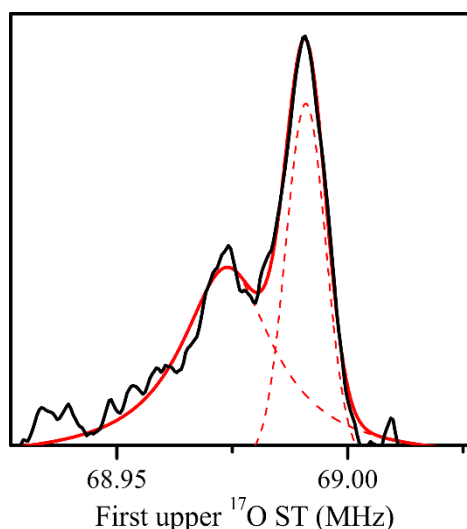
Supplementary Figure 4: Planar ^{63}Cu NQR vs. NMR satellite spectra for the magnetic field $B_0 \perp c$ along one Cu-O-Cu bond direction

The upper and lower panels correspond to 300 K and 100 K, respectively, with pressures of 0 kbar (a, d), 9 kbar (b, e) and 18 kbar (c, f). Vertical dashed lines indicate the calculated position expected for an axially symmetric EFG from zero field data. The NMR satellites (black) do not agree with what is expected from NQR measurements and an EFG asymmetry expected for orthorhombicity in a twinned crystal (green), cf. Methods in main article. For instance, the intensity mismatch (a, b, d) or the entire absence of an expected second line (f) is direct evidence against the orthorhombic scenario for the asymmetry of the planar Cu EFG. In particular the coincidence in (f) of the NMR satellite with only one, the upper green line shows alignment of Cu EFG throughout the twinned crystal, i.e., charge ordering.



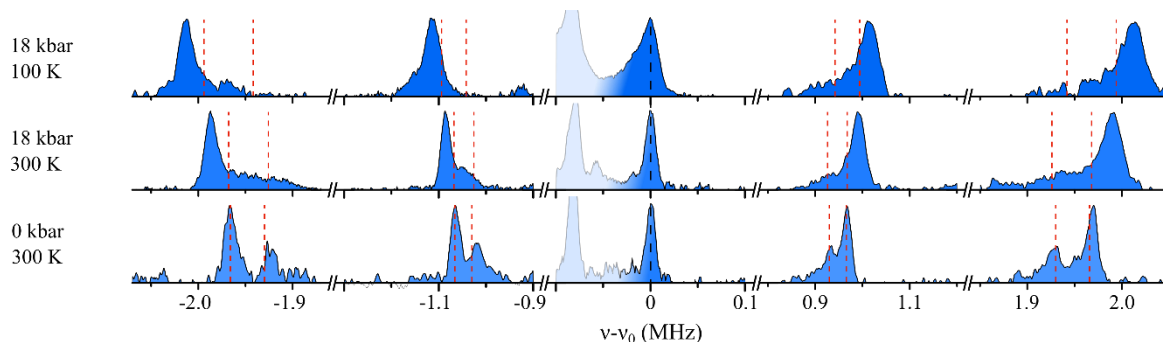
Supplementary Figure 5: Orthorhombicity and planar oxygen line splitting

(a) Monotonic increase of the orthorhombicity $(a-b)/(a+b)$ with doping (black). Also shown is the underdoped (stoichiometric) component $\text{YBa}_2\text{Cu}_4\text{O}_8$. Pressure (red) changes the orthorhombicity of optimally doped YBCO only slightly. (b) Difference of the planar oxygen quadrupole splittings of the two inequivalent sites O(2) and O(3) measured in $c \parallel B_0$ vs. orthorhombicity. Satellite splitting seems to occur only in well-ordered compounds and, although the orthorhombicity differs by a factor of two, the size of the splitting is similar in these materials. Interestingly, the total satellite linewidth is largely independent on whether a splitting is observed or not, cf. Fig. 8 in main article.



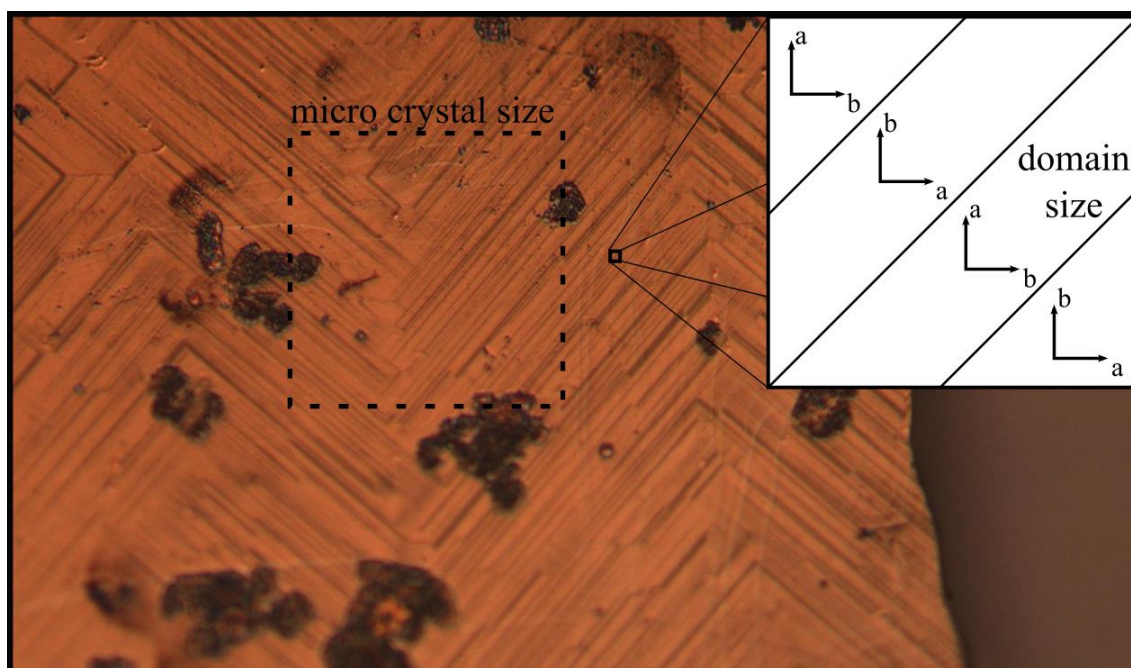
Supplementary Figure 6: ^{17}O satellite lineshape

The planar ^{17}O first high frequency satellite transition (black) at ambient pressure measured with the magnetic field along the Cu-O bond direction reveals only one sharp edge to higher quadrupole frequencies. Also shown is a fit of a distribution function (solid red) consisting of a Gaussian and Lorentzian line (dashed red) with roughly equal intensities. If solely two lines are present, they have different shapes, but also a more complex distribution could be present.

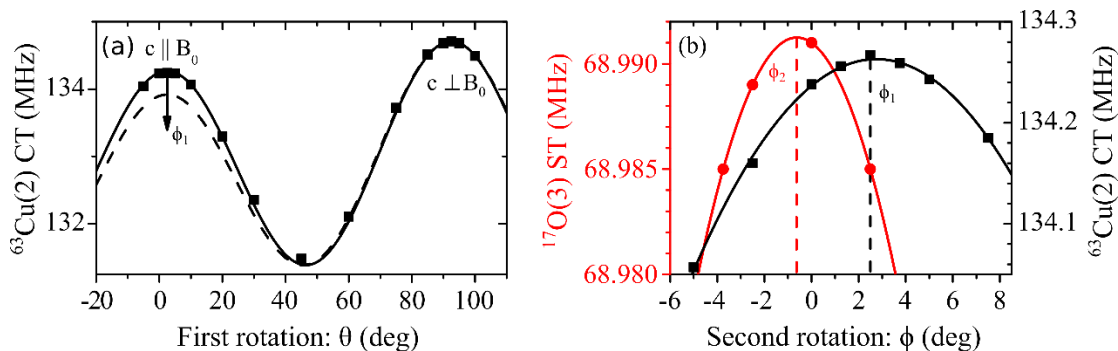


Supplementary Figure 7: Pressure and temperature dependence of planar ^{17}O spectra with the magnetic field $B_0 \perp c$ along one Cu-O-Cu bond direction

The magnetic frequency contribution was subtracted to emphasize the changes in the quadrupole splitting. Red dashed lines are the expectations using Laplace equation from the peak values of quadrupole splitting measured in the other two orientations, i.e., with the magnetic field perpendicular to the Cu-O-Cu bond and parallel to the c -axis. While we have agreement at ambient conditions, the pronounced differences at elevated pressure reflect local charge ordering. Transitions from other O sites are shaded.

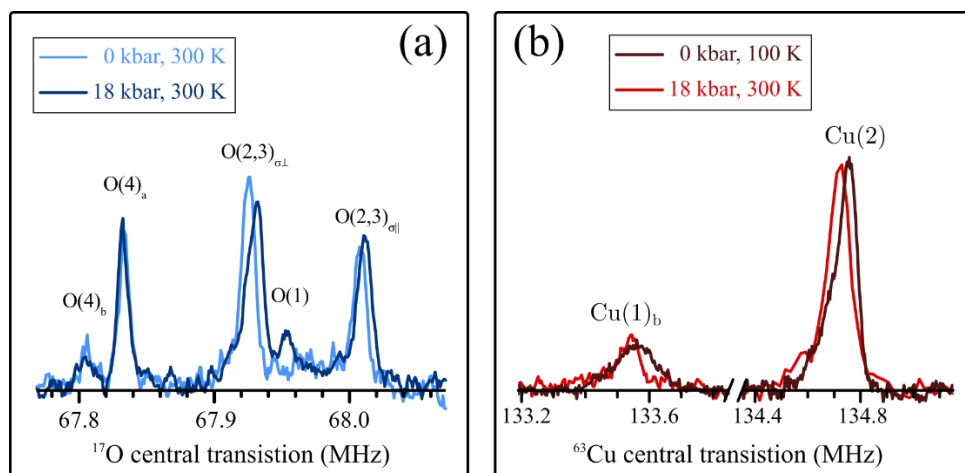


Supplementary Figure 8: Polarization microscopy image of a $\text{YBa}_2\text{Cu}_3\text{O}_7$ single crystal (Main panel) Twinning lines, which occur at the twin boundaries on the crystal's ab -plane, are visually enhanced using a polarization filter. A square of $150 \mu\text{m}$ illustrates the micro sample dimensions and numerous boundaries indicating equal occurrence of both orientations. (Inset) Pictogram of the visible twinning lines between domains ($1\text{-}3 \mu\text{m}$) and the corresponding orientation of the alternating crystal axes.



Supplementary Figure 9: Alignment of the crystal within the pressure cell using NMR

The single crystal is glued on the anvil and the assembled pressure cell is mounted on a two angle goniometer. The alignment of the crystal with respect to the external magnetic field was done using the angular dependence of the magnetic shift and quadrupole frequency. (a) ^{63}Cu central transition as a function of the first rotation angle θ exhibits two maxima. While one maximum corresponds to $c \perp B_0$, only if the rotation axis is perpendicular to the crystal's c -axis (solid line), the other maximum gives $c \parallel B_0$. A misalignment of $\Phi_1=10^\circ$ is shown by the dashed line demonstrating the good pre-orientation of the crystal. (b) Fine alignment using a second rotation axis which is perpendicular to the external magnetic field direction and the first rotation axis. For $c \parallel B_0$, another maximum appears for ^{63}Cu central transition at Φ_1 (black). Starting at $c \perp B_0$, the maximal frequency of the satellite transition of ^{17}O at Φ_2 is used to find B_0 along one Cu-O-Cu bond direction. The solid lines in (b) are parabolic fits.



Supplementary Figure 10: Unchanged twinning seen by apical O and chain Cu

(a) ^{17}O central transitions in $c \perp B_0$ without and with applied pressure. Signal intensity of apex oxygen measured along a and b axis unchanged by application of 18 kbar, showing that the crystal's twinning is unchanged. Signal intensity of $\text{O}(4)_b$ is suppressed by long spin-lattice relaxation time relative to short experimental repetition time.

(b) ^{63}Cu central transitions in $c \perp B_0$ of chain copper $\text{Cu}(1)_b$, measured along CuO-chain, and planar $\text{Cu}(2)$ without and with applied pressure. The integrated spectral intensity ratio $I_{\text{Cu}(2)}/I_{\text{Cu}(1)_b}$ is 3.5 at (0 kbar, 100 K) and 4.4 at (18 kbar, 300 K), consistent with the expected ratio of 4 for a twinned crystal rather than 2 for a de-twinned crystal. At (18 kbar, 300 K) suspected overlap of the central transition of $\text{Cu}(1)_a$ with $\text{Cu}(2)$ could explain the increased ratio since then the expected ratio would be $(I_{\text{Cu}(2)}+I_{\text{Cu}(1)_a})/I_{\text{Cu}(1)_b}=5$.